AIAA JOURNAL
Vol. 33, No. 4, April 1995

Technical Notes

TECHNICAL NOTES are short manuscripts describing new developments or important results of a preliminary nature. These Notes cannot exceed 6 manuscript pages and 3 figures; a page of text may be substituted for a figure and vice versa. After informal review by the editors, they may be published within a few months of the date of receipt. Style requirements are the same as for regular contributions (see inside back cover).

Computational Analysis of Buffet Alleviation in Viscous Transonic Flow over a Porous Airfoil

Mark A. Gillan*
Short Brothers, Belfast, Northern Ireland, BT3 9DZ, United Kingdom

Introduction

TRANSONIC flow past an airfoil at a high freestream Mach number is traditionally defined as consisting of large supersonic regions embedded within a subsonic flowfield. The pressure fluctuations initiated by the shock/boundary-layer interaction may excite intense levels of buffeting.[1] Therefore, to extend the buffet boundaries for a particular airfoil, a technique is required which is capable of controlling either the boundary layer, or alternatively, the shock strength.

Boundary-layer control may be performed by employing either blowing or suction within the interaction region. Blowing has a twofold effect, namely, an increase in the boundary-layer thickness coupled with a reduction in the skin friction, whereas suction induces a contrasting decrease in boundary-layer thickness and increase in skin friction. Passive control of the shock/boundary-layer interaction is a technique which provides a combination of blowing and suction forward and aft of the shock, respectively, without the need for a pump. A passive control device (Fig. 1) consists of a porous region and plenum which are positioned at the interaction region. The static pressure rise across the shock wave results in the flow traveling through the plenum to the region of lower pressure forward of the shock position. The increased communication across the shock stimulates the development of a thicker boundary layer forward of the shock. This process effectively changes the airfoil's geometry in a manner which produces a weaker lambda shock system. Moreover, passive control's inherent damping characteristics have been shown experimentally[2-5] to reduce the pressure fluctuations initiated by the shock/boundary-layer interaction and, therefore, delay buffet onset.

In the present study, time-accurate flow over an 18%-thick porous circular-arc airfoil is computed in an attempt to ascertain whether passive control will damp, or even eliminate, the flow periodicity detected in the corresponding solid airfoil (CSA) computation,[6] thus extending the airfoil's buffet boundary. The following sections briefly describe both the numerical procedure and the results.

Numerical Model

An explicit Navier–Stokes finite volume scheme MGENS has been developed which is capable accurately predicting viscous flow over an arbitrary airfoil using an orthogonal boundary conforming hyperbolic grid MGHYPR. A detailed description of both the Navier–Stokes code and the grid generation scheme is given in Ref. 6.

The two-dimensional mass-averaged Navier–Stokes equations may be written in integral form as

$$\frac{\partial}{\partial t}\iint_{\Omega} \boldsymbol{W} d\Omega + \int_{\partial\Omega} \bar{\boldsymbol{F}}\cdot\boldsymbol{n}\, ds = 0 \tag{1}$$

where Ω, $\partial\Omega$, $\boldsymbol{W}$ and $\bar{\boldsymbol{F}}$ are the region of interest, the boundary curve, the vector of conserved quantities, and the flux tensor, respectively. The governing equations are firstly discretized in space using a second-order cell-vertex-centered differencing formulation. An explicit five-stage Runge–Kutta time-stepping scheme is then employed to advance the equations to a second-order time-accurate solution. High-frequency damping and clean shock capturing are achieved by adaptive artificial dissipation. Adiabatic no-slip conditions are assumed at solid wall boundaries, whereas the nonreflecting far-field boundary, which is located at approximately 20 chord lengths from the airfoil's surface, is constructed using Riemann invariants. Time-accurate implicit residual smoothing with variable coefficients and a three-level saw-tooth multigrid scheme facilitate convergence. Finally, turbulence closure is performed using the algebraic Baldwin–Lomax model.[7] A comprehensive set of validation results is presented in Ref. 6, for both steady and periodic flows over solid airfoils. These results are in excellent agreement with contemporary numerical studies using similar turbulence models.

Darcy's Law

To date every computational investigation involving passive control modeling has utilized Darcy's law to simulate the porous surface flow characteristics, whereby the velocity of a fluid, through a given medium, is assumed to be directly proportional to the pressure drop across that medium. In nondimensional form, Darcy's law may be written as

$$v_n = -\bar{\sigma}\,\Delta p$$

where

$$\Delta p = (p_{\text{wall}} - \bar{p}) \tag{2}$$

with v_n, p_{wall}, $\bar{p}$, and $\bar{\sigma}$ representing the transpiration velocity at the porous surface, the wall pressure, the plenum pressure, and the porosity distribution function, respectively. The porosity distribution function $\bar{\sigma}$ is dependent on both the fluid viscosity and the porous surface configuration.

The constant plenum pressure $\bar{p}$ is determined from an application of the conservation of mass at the porous surface, namely,

$$\int_s \rho_{\text{wall}} v_n\, ds = 0 \tag{3}$$

Substituting for v_n, using Eq. (2), the preceding expression gives

$$\bar{p} = \frac{\int_s \rho_{\text{wall}} p_{\text{wall}}\, ds}{\int_s \rho_{\text{wall}}\, ds} \tag{4}$$

The transpiration velocity v_n may now be calculated using Eq. (2) in conjunction with the given definition for the plenum pressure $\bar{p}$.

Received June 8, 1993; presented as Paper 93-3419 at the AIAA 11th Applied Aerodynamics Conference, Monterey, CA, Aug. 9–13, 1993; revision received April 14, 1994; accepted for publication May 2, 1994.

*Research Technical Engineer, Nacelle Systems. Member AIAA.

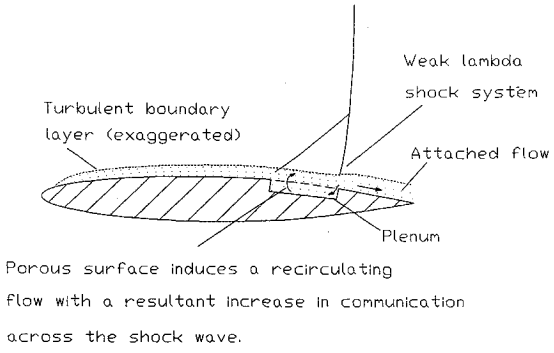

Fig. 1 Transonic flow past a porous airfoil.

Two important assumptions are made in the derivation of Darcy's law which relate mainly to the proposed existence of laminar flow within the plenum. Indeed, the direct proportionality which exists between the transpiration velocity and the change in pressure [Eq. (2)] is entirely consistent with inherently laminar flow regimes.

The first major computational restriction which is imposed on the numerical scheme refers to the magnitude of the velocities allowed in the plenum which, in turn, governs the transpiration velocities at the porous surface. In general, the porosity distribution function is modified until the transpiration velocities are less than 5% of the freestream flow velocity U_∞

$$\left|\frac{v_n}{U_\infty}\right| \leq 0.05 \tag{5}$$

Second, the plenum, which is constrained to be narrow with a corresponding high aspect ratio, is also deemed to have a constant pressure $\bar{p}$. Extensive investigations into the effects that variable plenum dimensions have on the internal flow structure were performed by Lamar,[8] Brandeis,[9] and Kim and Chokani.[10] They detected the existence of unsteady/periodic pressure fluctuations within the plenum, over a wide range of aspect ratios. Therefore, it is unlikely that the plenum pressure $\bar{p}$ will remain strictly constant along its length for any given aspect ratio. However, it is not inconceivable to imagine the development of a control device which would enforce this condition. Hence, whereas the term passive control will be maintained in the ensuing analysis, a certain degree of active control would be required to physically reproduce the porous surface computations presented.

Code Modifications

The introduction of a transpiration velocity distribution on the airfoil's surface, due to the presence of a porous region, has necessitated a partial recoding of the wall boundary conditions in addition to redefining the damping constant A^+.

The no-slip condition, which is enforced at the wall, is now invalid in the vicinity of the porous region. Furthermore, the change in pressure in the η direction (of the ξ-η computational domain) is strictly no longer negligible at the porous surface. However, as indicated by previous authors[11] the orthogonality of the grid with respect to the porous surface, coupled with the enforcement of a more stringent high Reynolds number approximation whereby an extremely small initial normal cell height is employed ($y^+ < 2$), implies that

$$\left(\frac{\partial(\boldsymbol{U}\cdot\boldsymbol{n})}{\partial\eta}\right)_{\text{wall}} \approx 0, \qquad \text{hence} \qquad \left(\frac{\partial p}{\partial\eta}\right)_{\text{wall}} \approx 0 \tag{6}$$

where $\boldsymbol{U}$ and $\boldsymbol{n}$ are the velocity and unit normal vectors, respectively. Therefore, a one-dimensional jet flow in the $\xi = k$ direction is assumed for the initial cells located along the porous region. Hence, formulation of the porous wall boundary conditions remains exactly as cited earlier with the exception that the no-slip condition is replaced with a transpiration velocity v_n.

Finally, in its present formulation, the Baldwin–Lomax turbulence model does not take into account the effects of localized blowing and suction in the vicinity of the porous region. In an attempt to introduce these mass-transfer effects, the damping constant A^+ is redefined as

$$A^+ = 26.0\, e^{(-5.9 v_n^+)}$$

where

$$v_n^+ = \frac{v_n}{(\tau_{\text{wall}}/\rho_{\text{wall}})^{\frac{1}{2}}} \tag{7}$$

with τ_{wall} denoting the wall shear stress. The modification, which was first employed by Chokani and Squire,[12] effectively decreases A^+ when blowing (positive v_n) is being performed, with a corresponding increase in the mass-transfer rate. However, suction (negative v_n) increases A^+ which, in turn, induces a relatively more laminarized flowfield.

Results and Discussions

Periodic Transonic Viscous Flow over a Porous 18%-Thick Circular-Arc Airfoil

Time-accurate transonic viscous flow was computed over a porous 18%-thick circular-arc airfoil, at 0-deg angle of attack, with a freestream Mach number of $M_\infty = 0.771$ and a Reynolds number of $Re_\infty = 11 \times 10^6$. This passive control investigation represents a continuation of the CSA computation performed in Ref. 6, which produced periodic Tijdeman-type[13] B SIO with a reduced frequency of $k = 0.396$ (see Fig. 2). Although this reduced frequency is approximately 21% lower than that obtained by McDevitt et al.,[14] it compares extremely favorably with the computed values of 0.4 and 0.406 obtained by Levy[15] and Edwards and Thomas,[16] respectively.

The porous surface region was located from $x_1 = 0.504c$ to $x_2 = 0.770c$, on both the upper and lower surfaces. Moreover, a porous distribution function of $\bar{\sigma} = 0.4$ was employed which induced transpiration velocities of less than 5% of the freestream velocity U_∞, thereby satisfying Eq. (5). A 320 × 64 cell orthogonal boundary-conforming hyperbolic C grid was employed, with 256 cells placed on the airfoil's surface. The far-field boundary was located at 20 chord lengths, with the initial near-wall normal grid spacing corresponding to a value of $y^+ < 2$. Therefore, this cell spacing satisfies the solid wall high Reynolds number approximation ($y^+ < 5$), in addition to the more demanding porous surface approximation.

The porous computation was performed using the periodic solution obtained from Ref. 6 (see Fig. 2) as the initial conditions. Nearly 40,000 multigrid iterations were performed, corresponding to approximately 42.05 nondimensional time (NDT) units. During this time the CSA would have traveled almost 39 chord lengths. Because of the symmetrical nature of this investigation only the upper surface flowfield characteristics are discussed.

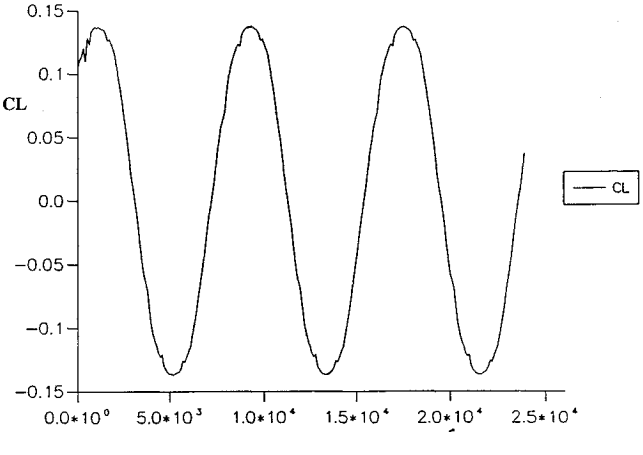

Fig. 2 Lift coefficient time history plot for solid circular-arc airfoil at $\alpha = 0$ deg, $M_\infty = 0.771$, and $Re_\infty = 11.0 \times 10^6$.

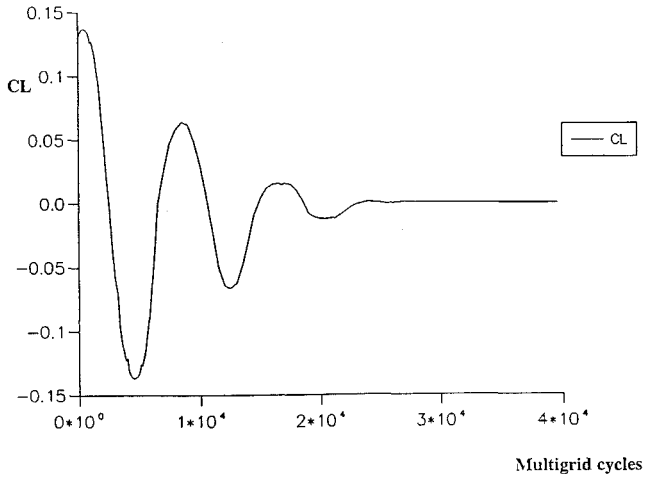

Fig. 3 Lift coefficient time history plot for circular-arc airfoil with porous configuration $\bar{\sigma}$ = 0.4, x_1 = 0.504c, x_2 = 0.770c at α = 0 deg, M_∞ = 0.771, and Re_∞ = 11.0 × 10⁶.

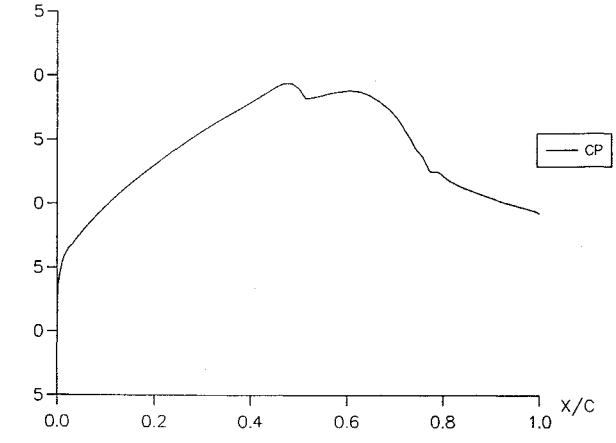

Fig. 4 Pressure coefficient plot for circular-arc airfoil with porous configuration $\bar{\sigma}$ = 0.4, x_1 = 0.504c, x_2 = 0.770c at α = 0 deg, M_∞ = 0.771, and Re_∞ = 11.0 × 10⁶.

The resultant lift coefficient time history plot (Fig. 3) indicates that after approximately 28,000 cycles, or 29.44 NDT, a steady-state solution is obtained. The periodic Tijdeman-type B SIO, which was present for the CSA configuration, has therefore been damped and eventually eliminated from the now steady flowfield. Interestingly, the period of the oscillation remains unaltered throughout the damping process, despite significant decreases in amplitude between successive oscillations.

The corresponding pressure coefficient plot (Fig. 4) is characteristic of those presented earlier. Referring to Fig. 4 passive control appears to have captured the SIO, with a resultant dramatic decrease in the pressure gradient, due to the introduction of a weak lambda shock system. The leading leg of the lambda shock is positioned at the start of the porous region, with the second normal leg located at the rear. Furthermore, a large reduced pressure/separation region is detected aft of the porous surface. These flow phenomena, in addition to the symmetrical nature of the resultant flowfield, are clearly illustrated in the Mach contour plot (Fig. 5). At approximately 50% chord an initial shock is detected, which corresponds to the lambda shock's leading leg. The flow then recovers slightly in the presence of a favorable pressure gradient, up until 77% chord where the lambda shock's second leg retards the flow once more. Aft of this location the flow separates which is in marked contrast to the alternating separated (up to 40% chord)/attached flow exhibited by the CSA.

Passive control, therefore, acts as a damping device due to the enforcement of a constant pressure within the plenum $\bar{p}$, which effectively prohibits the evolution of a periodic flow. Therefore, unsteady

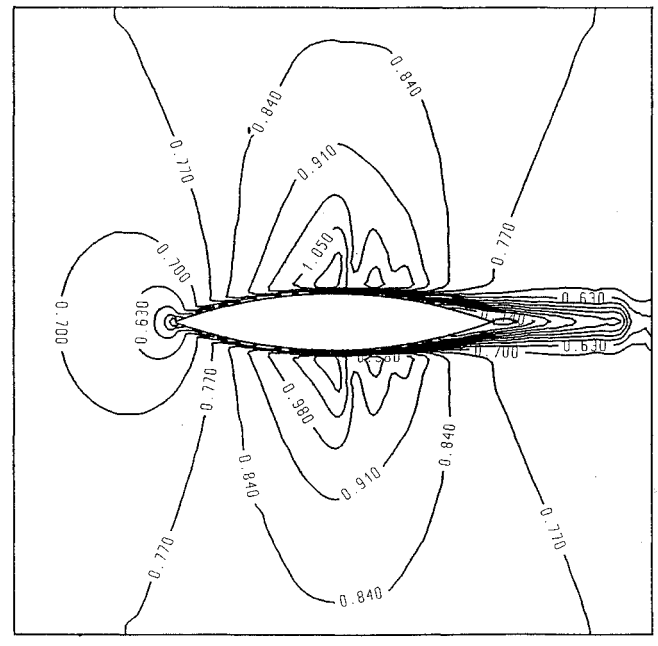

Fig. 5 Mach contour plot for circular-arc airfoil with porous configuration $\bar{\sigma}$ = 0.4, x_1 = 0.504c, x_2 = 0.770c at α = 0 deg, M_∞ = 0.771, and Re_∞ = 11.0 × 10⁶.

phenomenon, such as buffet, have been temporarily removed from the transonic flowfield. However, as cited earlier, a certain degree of active control would be required to maintain a constant plenum pressure. This could possibly be achieved by lining the plenum's surface with a pressure sensitive material, which is capable of deforming in a manner that would equalize the interior pressure. Furthermore, the development of a steady flowfield may also be attributed to an effective ramp change in the airfoil's profile, due to the introduction of transpiration velocities in the locality of the porous region. This ramp change is responsible for the development of a lambda shock system on both the upper and lower surfaces. The resultant flowfield characteristics, due to the formation of the lambda system, are no longer consistent with those exhibited within the small periodic band, as detected in Ref. 6, thereby inducing a steady flowfield.

Concluding Remarks

A computational investigation into the effects of passive control on periodic transonic viscous flow over an 18%-thick circular-arc airfoil has been presented. To perform this analysis, an explicit finite volume cell-vertex-centered Navier–Stokes solver has been developed, in conjunction with an orthogonal boundary conforming hyperbolic C-grid generator. The ability of passive control to suppress Tijdeman-type-B SIO, which invariably leads to buffet, has been demonstrated for the first time using a Navier–Stokes solver.

References

[1]Seegmiller, H. L., Marvin, J. G., and Levy, L. L., Jr., "Steady and Unsteady Transonic Flow," *AIAA Journal*, Vol. 16, No. 12, 1978, pp. 1262–1270.

[2]Krogmann, P., Stanewsky, E., and Thiede, P., "Effects of Local Boundary Layer Suction on Shock/Boundary-Layer Inter-action and Shock-Induced Separation," AIAA Paper 84-0098, 1984.

[3]Raghunathan, S., "Pressure Fluctuation Measurements with Passive Shock Wave Boundary Layer Control," *AIAA Journal*, Vol. 25, No. 4, 1987, pp. 626–628.

[4]Raghunathan, S., and Mabey, D. G., "Buffet Breathers for Aerofoils," U.K. Patent Application No. 8600175, 1986.

[5]Hall, D. E., "Alleviation of Shock Oscillations in Transonic Flow by Passive Controls," Ph.D. Thesis, Aeronautical Engineering Dept., Queen's Univ. of Belfast, Belfast, Northern Ireland, UK, 1991.

[6]Gillan, M. A., "A Computational Analysis of Viscous Flow Over Porous Aerofoils," Ph.D. Thesis, Aeronautical Engineering Dept., Queen's University of Belfast, Belfast, Northern Ireland, UK, 1993.

[7]Baldwin, B. S., and Lomax, H., "Thin Layer Approximation and Algebraic Model for Separated Turbulent Flows," AIAA Paper 78-257, 1978.
[8]Lamer, W. E., "Effects of Buffeting and Other Transonic Phenomena," AGARD-CP-187, 1976.
[9]Brandeis, J., "Flow Separation in Shear-Layer-Driven Cavities," *AIAA Journal*, Vol. 20, No. 7, 1981, pp. 908–914.
[10]Kim, I., and Chokani, N., "Navier–Stokes Study of Supersonic Cavity Flowfield with Passive Control," *Journal of Aircraft*, Vol. 29, Feb. 1992, pp. 217–223.
[11]Chen, C. L., Chow, Y. C., Van Dalsem, W. R., and Holst, T. L., "Computation of Viscous Transonic Flow Over Porous Airfoils," *Journal of Aircraft*, Vol. 26, Dec. 1989, pp. 1067–1075.
[12]Chokani, N., and Squire, L. C., "Passive Control of Shock/Boundary Layer Interactions: Numerical and Experimental Studies," *Symposium Transsonicum III*, Gottingen, Germany 1989, pp. 24–27.
[13]Tijdeman, H., "Investigation of the Transonic Flow Around Oscillating Airfoils," National Aerospace Lab., NLR TR-77-090U, The Netherlands, 1977.
[14]McDevitt, J. B., Levy, L. L., Jr., and Deiwert, G. S., "Transonic Flow About a Thick Circular-Arc Airfoil," *AIAA Journal*, Vol. 14, No. 5, 1976, pp. 606–613.
[15]Levy, L. L., Jr., "Experimental and Computational Steady and Unsteady Transonic Flows About a Thick Airfoil," *AIAA Journal*, Vol. 16, No. 6, 1978, pp. 564–572.
[16]Edwards, J. W., and Thomas, J. L., "Computational Methods for Unsteady Transonic Flows," *Unsteady Transonic Aerodynamics*, edited by D. Nixon, Vol. 120, Progress in Astronautics and Aeronautics, AIAA, Washington, DC, 1989, pp. 211–261.

Rise of Total Pressure in Frictional Flow

R. I. Issa*
Imperial College,
London SW7 2BX, England, United Kingdom

Introduction

ONE of the first basic principles introduced to students of fluid mechanics is Bernoulli's equation and its consequence on the conservation of total pressure in inviscid flow. Flows with friction, on the other hand, are known to result in a net loss of total pressure. Such loss, however, is always considered in the context of global changes occurring over macroscopic control volumes that are of interest in normal engineering applications. Thus, many if not most practitioners of fluid mechanics have come to assume that total pressure is an upper-bounded quantity, being conserved in inviscid flow, and can only decrease in frictional flow.

With the advent of modern computational methods for solving the Navier–Stokes equations, full flowfield calculations are now commonplace. In many of these computations, which often incorporate models accounting for turbulence, values of the total pressure, especially around stagnation points in external aerodynamics and on blades in cascades, have been observed to be higher than the corresponding incident freestream values. This occurs even in highly turbulent flows, when frictional effects are expected to substantially reduce total pressure. Such increase has hitherto been assumed to be due to numerical errors contaminating the solution.

In this Note, it is shown that the expectation that total pressure in frictional flow is everywhere bounded by a maximum value that equals that of the incident freestream is in fact erroneous. It is reasoned and demonstrated that the total pressure can indeed increase locally, especially around stagnation points, beyond the freestream value. It is also shown that, surprisingly, this increase is directly proportional to the viscosity.

The analysis offered here first derives a transport equation for total pressure from the Navier–Stokes equations; such an equation appears in standard text books like Ref. 1 where it is pointed out that gradients in stresses in the equation result in gradients in total pressure. It is argued here that these stress gradients can indeed act as a positive source. Two known exact solutions to the Navier–Stokes equations, namely, those of plane stagnation flow and Stokes flow around a sphere, are then considered. The exact solutions for the total pressure fields for these cases are then formulated and presented.

Received Feb. 22, 1994; revision received May 3, 1994; accepted for publication May 3, 1994.

*[Job Title] Department of Mechanical Engineering.

Governing Equations

We first examine in general the variations of total pressure as governed by the transport equations. Consider the momentum equations in multidimensions for an incompressible fluid. In Cartesian tensor notation these can be written as

$$\frac{\partial}{\partial x_j}(\rho u_j u_i) = -\frac{\partial p}{\partial x_i} + \frac{\partial \sigma_{ij}}{\partial x_j} \tag{1}$$

where σ_{ij} is the stress tensor. Multiplication of Eq. (1) by u_i gives

$$u_i \frac{\partial}{\partial x_j}(\rho u_j u_i) = -u_i \frac{\partial p}{\partial x_i} + u_i \frac{\partial \sigma_{ij}}{\partial x_j} \tag{2}$$

which can be reformulated as

$$\frac{\partial}{\partial x_j}\left(\rho u_j \frac{u_i u_i}{2}\right) = -\frac{\partial}{\partial x_i}(u_i p) + u_i \frac{\partial \sigma_{ij}}{\partial x_j} \tag{3}$$

In arriving at Eq. (3), the continuity condition for incompressible fluids

$$\frac{\partial u_i}{\partial x_i} = 0$$

has been invoked. Equation (3) can be rearranged to give

$$\frac{\partial}{\partial x_j}\left[u_j\left(p + \rho\frac{u_i u_i}{2}\right)\right] = u_i \frac{\partial \sigma_{ij}}{\partial x_j}$$

or

$$\frac{\partial}{\partial x_j}(u_j p_t) = u_i \frac{\partial \sigma_{ij}}{\partial x_j} \tag{4}$$

where the total pressure p_t is defined as

$$p_t = p + \rho\frac{u_i u_i}{2}$$

Equation (4) is a transport equation governing the total pressure. In inviscid flow, the right-hand side of the equation vanishes, thus dictating that the total pressure is constant along each streamline.

In viscous flow, however, the right-hand side of Eq. (4) can, in principle, lead to an increase in total pressure, depending on the sign of the term, which can be written as

$$u_i \frac{\partial \sigma_{ij}}{\partial x_j} = \underbrace{\frac{\partial}{\partial x_j}(u_i \sigma_{ij})}_{\text{I}} - \underbrace{\sigma_{ij}\frac{\partial u_i}{\partial x_j}}_{\text{II}} \tag{5}$$

Term II in Eq. (5) stands for dissipation and will always act as a negative source. Term I, however, is a redistribution term and can be either positive or negative.

If one integrates Eq. (4) over the flow domain, the integral of term I vanishes when no work is imparted to the fluid at the boundaries. Term II will always have a negative sign, hence leading to a net loss of total pressure over the domain. There is no reason, however, why locally term I should not be positive and greater in magnitude than term II, thereby giving a local rise in total pressure. This rise can only happen at the expense of depletion of total pressure eleswhere in the flow as mechanical energy is redistributed due to the stresses.

In what follows, the previous conjecture is verified by consideration of two flows for which analytic solutions exist.